Quantum-dot-tagged microbeads for multiplexed optical coding of biomolecules

Mingyong Han, Xiaohu Gao, Jack Z. Su, and Shuming Nie*

Multicolor optical coding for biological assays has been achieved by embedding different-sized quantum dots (zinc sulfide–capped cadmium selenide nanocrystals) into polymeric microbeads at precisely controlled ratios. Their novel optical properties (e.g., size-tunable emission and simultaneous excitation) render these highly luminescent quantum dots (QDs) ideal fluorophores for wavelength-and-intensity multiplexing. The use of 10 intensity levels and 6 colors could theoretically code one million nucleic acid or protein sequences. Imaging and spectroscopic measurements indicate that the QD-tagged beads are highly uniform and reproducible, yielding bead identification accuracies as high as 99.99% under favorable conditions. DNA hybridization studies demonstrate that the coding and target signals can be simultaneously read at the single-bead level. This spectral coding technology is expected to open new opportunities in gene expression studies, high-throughput screening, and medical diagnostics.

Recent advances in bioanalytical sciences and bioengineering have led to the development of DNA chips[1,2], miniaturized biosensors[3,4], and microfluidic devices (e.g., microelectromechanical systems or bioMEMS)[5–7]. These enabling technologies have substantially influenced many areas in biomedical research, such as gene expression profiling, drug discovery, and clinical diagnostics. As current research in genomics and proteomics produces more sequence data, there is a need for technologies that can rapidly screen a large number of nucleic acids and proteins. Here we report the development of optically encoded microbeads (1.2 μm) for massively parallel and high-throughput analysis of biological molecules. This encoded-bead technology is based on the optical properties of semiconductor QDs (refs 8,9) and our ability to incorporate multicolor QDs into small polymer beads at precisely controlled ratios. A surprising finding is that the embedded QDs are spatially separated from each other and do not undergo fluorescence resonance energy transfer.

The basic concept is to develop smart microstructures that have not only molecular recognition abilities but also built-in codes for rapid target identification. For example, the surface of a polymer bead can be conjugated to biomolecular probes such as oligonucleotides and antibodies, while an identification code is embedded in the bead's interior. By integrating molecular recognition and optical coding, each bead could be considered a "chemical lab" that detects and analyzes a unique sequence or compound in a complex mixture. Such encoded beads should find broad application in gene expression studies, high-speed screening, and medical diagnostics. In comparison with planar DNA chips, encoded-bead technology is expected to be more flexible in target selection (e.g., adding new genes or single-nucleotide mutations[10]), faster in binding kinetics (similar to that in homogeneous solution), and less expensive to produce.

A major problem with the encoded-bead approach, however, is that no technologies are currently available for massively parallel coding on the nanometer or micrometer scale. In this paper, we show that this problem can be solved by exploiting the optical properties of semiconductor QDs such as ZnS-capped CdSe nanocrystals. Previous studies have used water-soluble QDs as biological labels[11–15]; here we have embedded *hydrophobic* QDs into polymer beads for high-capacity spectral coding. These luminescent QDs are ideal fluorophores for this purpose because their fluorescence emission wavelength can be continuously tuned by changing the particle size, and a single wavelength can be used for simultaneous excitation of different-sized QDs (refs 8,9). In addition, surface-passivated QDs are highly stable against photobleaching and have narrow, symmetrical emission peaks (25–30 nm full width at half maximum).

Figure 1A illustrates the principles of multiplexed optical coding based on multicolor semiconductor QDs. The use of 10 intensity levels (0, 1, 2, ... 9) at a single wavelength (color) gives 9 unique codes ($10^1 - 1$), because level "0" cannot be differentiated from the background. The number of codes increases exponentially when multiple wavelengths and multiple intensities are used at the same time. For example, a 3-color/10-intensity scheme yields 999 codes ($10^3 - 1$), whereas a 6-color/10-intensity scheme has a theoretical coding capacity of about one million. In general, n intensity levels with m colors generate ($n^m - 1$) unique codes. However, the actual coding capabilities are likely to be substantially lower because of spectral overlapping, fluorescence intensity variations, and signal-to-noise requirements. Preliminary studies in our group suggest that it is better to use more colors, rather than more intensity levels, in order to increase the number of usable codes. Figure 1B shows 10 distinguishable fluorescence-emission colors observed from QDs excited with a near-UV (350 nm) lamp. A realistic scheme could use 5–6 colors with 6 intensity levels (0, 1, … 5), yielding approximately 10,000 to 40,000 recognizable codes.

The potential of multiplexed coding (e.g., using multiple wavelengths and multiple intensities) has been recognized by other researchers. Fulton *et al.* used two organic dyes to encode a set of ~100 beads for multiplexed and multianalyte bioassays[16]. Walt and co-workers reported randomly ordered fiber-optic microarrays based on fluorescently encoded microspheres[17–19]. However, these previous studies were based on organic dyes and lanthanide complexes, and were limited by the unfavorable absorption and emission properties of these materials (e.g., inability to excite more than two or three fluorophores, broad and asymmetrical emission profiles, and spectral overlapping). Multicolor optical coding using lumines-

*Department of Chemistry, Indiana University, Bloomington, IN 47405. *Corresponding author (nie@indiana.edu).*

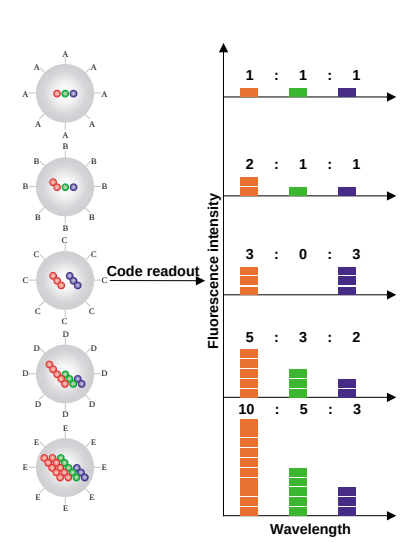

Figure 1. (A) Schematic illustration of optical coding based on wavelength and intensity multiplexing. Large spheres represent polymer microbeads, in which small colored spheres (multicolor quantum dots) are embedded according to predetermined intensity ratios. Molecular probes (A–E) are attached to the bead surface for biological binding and recognition, such as DNA–DNA hybridization and antibody–antigen/ligand–receptor interactions. The numbers of colored spheres (red, green, and blue) do not represent individual QDs, but are used to illustrate the fluorescence intensity levels. Optical readout is accomplished by measuring the fluorescence spectra of single beads. Both absolute intensities and relative intensity ratios at different wavelengths are used for coding purposes; for example (1:1:1) (2:2:2), and (2:1:1) are distinguishable codes. (B) Ten distinguishable emission colors of ZnS-capped CdSe QDs excited with a near-UV lamp. From left to right (blue to red), the emission maxima are located at 443, 473, 481, 500, 518, 543, 565, 587, 610, and 655 nm.

cent QDs offers important advantages and applications that are not possible with organic dyes or lanthanide probes. It is worth noting that radiofrequency (RF) encodable microchips are currently under development for multiplexed DNA assays and combinatorial chemical synthesis[20,21]. But these microfabricated devices have typical dimensions of 500 μm × 500 μm × 500 μm, and their volumes are about 70 million times larger than the 1.2-μm encoded beads reported in this paper.

Results and discussion

Using single-color QDs, we systematically investigated the conditions for incorporating them into polymer microbeads. The results reveal that cross-linked beads, formed by emulsion polymerization of styrene, divinylbenzene, and acrylic acid, are well suited for QD incorporation. By using a series of five QD samples synthesized according to published procedures[22–24], we prepared single-color coded beads with emission wavelengths that were nearly identical to those of the original QDs. Figure 2 shows a multicolor fluorescence image obtained from a mixture of these beads spread on a glass surface. It is important to note that a true-color digital camera and a single light source were used in this experiment. Remarkably, all the coded beads are observed, and their emission colors are clearly distinguishable. As noted earlier, this type of simultaneous excitation is not possible with fluorescent microspheres containing organic dyes. Confocal imaging studies indicate that the QDs are mainly located in the outer 25% of the bead's radius, similar to the spatial distribution of organic dyes in polystyrene beads[25]. However, this determination is only an approximate estimate because the microbeads refract light and cause image distortion.

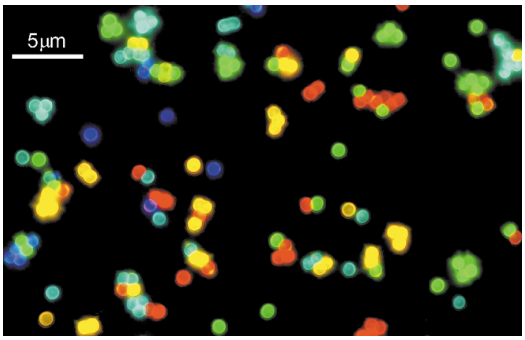

Figure 2. Fluorescence micrograph of a mixture of CdSe/ZnS QD-tagged beads emitting single-color signals at 484, 508, 547, 575, and 611 nm. The beads were spread and immobilized on a polylysine-coated glass slide, which caused a slight clustering effect. See Experimental Protocol for detailed conditions.

A key question is whether the embedded QDs would aggregate and couple with each other inside the beads, which could cause spectral broadening, wavelength shifting, and energy transfer. To our surprise, the fluorescence spectra of QD-tagged beads are narrower by ~10% than those of free QDs, and the emission maxima remain unchanged. We believe that the bead's porous structure acts as a matrix to spatially separate the embedded QDs, and also as a filter to block the incorporation of large particles and aggregates in a heterogeneous population. Our calculation indicates that the average distance between two adjacent QDs is ~30 nm within a 1.2-μm bead that contains 50,000 QDs (~0.1% vol/vol, corresponding to the maximum level of QD incorporation). Despite the uneven nature of QD distribution within the beads, this calculation suggests that the average separation distance is much larger than the Förster energy transfer radius (R_o = 5–8 nm) for QDs (refs 26,27).

Figure 3A, B shows quantitative and statistical data concerning the number of QDs per bead and the fluorescence intensity levels for coding. The number of QDs per bead is calculated by dividing the total number of QDs by the total number of beads in the mixture, under the assumption that the incorporation process is complete (i.e., no free QDs left in the supernatant). Fluorescence measurement confirmed the validity of this assumption for low-to-medium loading levels (<40,000 QDs per bead). As an independent measure, the fluorescence intensities of single QDs and single beads under identical experimental conditions were recorded. As mentioned above, the embedded QDs have similar optical properties as free QDs, and the ratio of these two intensities is approximately equal to the number of QDs per bead. Significantly, these two independent measurements yielded nearly identical results, establishing a linear relationship between the measured fluorescence intensity and the number of embedded QDs (Fig. 3A). This linear relationship further confirms the lack of fluorescence resonance energy transfer among the embedded QDs, a key requirement for multiplexed optical coding.

The uniformity and reproducibility of the tagged beads were analyzed by examining the variations of single-bead signals and by plotting histograms for each of the 10 intensity levels. As shown in Figure 3A, the small spreads (error bars) in the measured fluorescence intensities indicate a high level of bead uniformity. The relative

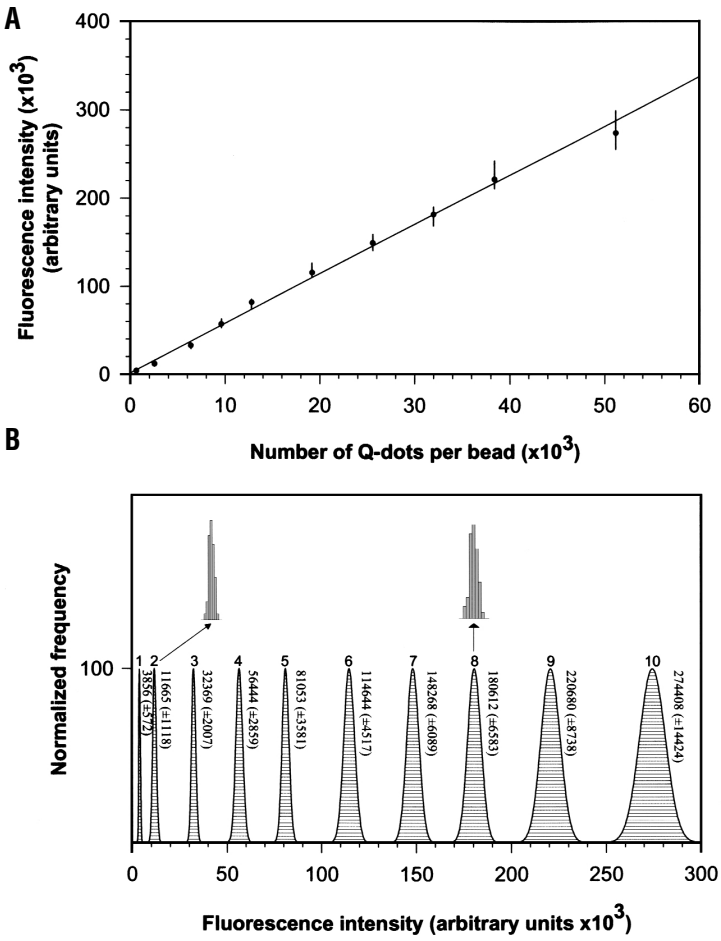

Figure 3. Quantitative analysis of single-bead signal intensities, uniformity and reproducibility of QD incorporation. (A) Relationship between the fluorescence intensity of a single bead and the number of embedded QDs. Each data point is the average value of 100–200 measurements, and the signal intensity spread (minimum to maximum) is indicated by an error bar. The first point (lowest intensity) corresponds to ~640 dots per bead. The last point shows a significant deviation from the linear line because of incomplete incorporation of QDs into the beads at this loading level. (B) Histogram plots for 10 intensity levels corresponding to the data points in (A). On the right side of each curve is shown the average fluorescence intensity as well as the standard deviation (in parentheses). Representative raw data are shown for levels 2 and 8.

standard deviations are about 10–15% at low-intensity levels, and decrease to about 3–5% at high-intensity levels. A major source of the errors appears to be the intrinsic variation in bead size (2–3% in diameter), as dictated by the emulsion polymerization procedure. Other contributing factors include variations in QD incorporation, shot noise (especially when the number of QDs per bead is small), and bead-positioning errors during data acquisition (this can be minimized by using an automated microfluidic device or flow cytometer). Even in the presence of these errors, the histograms in Figure 3B reveal that there is no intensity overlap among the first six levels at four standard deviations ($\pm 4\sigma$), and no overlap among the last four levels at three standard deviations ($\pm 3\sigma$). Thus, we estimate that the bead identification accuracies are as high as 99.99% for the first six intensity levels, and ~99.74% for the remaining four levels. These values are statistical accuracies for identifying single beads of different intensity levels, not the precision or reproducibility in measuring the absolute fluorescence intensities. Previously, Wild and co-workers have shown that only 500 photons are needed to assign a single fluorescent molecule to one of four species with a confidence level of 99.9% (ref. 28).

Following these single-color studies, we prepared multicolor QD-tagged beads, conjugated these beads to biomolecules, and carried out preliminary biological assays. Monodispersed QDs with fluorescence emission at the three primary colors (red, green, and blue) were synthesized, and were sequentially incorporated in polymer beads at precisely controlled ratios. For this procedure to be successful, the distribution of pore sizes within the beads must be carefully controlled, and the largest QDs (red) must be loaded first, followed by the medium (green) and small (blue) QDs in a sequential manner. Figure 4A shows a color image of these triple-color fluorescent beads together with a number of single-color beads. A striking feature is that the triple-color beads appear "white", because of a precise balance of the emission intensities for all three colors. This balance was achieved by controlling the proportions of different-sized QDs. Single-bead spectroscopy confirmed that the three fluorescence peaks have nearly identical intensities (Fig. 4B). In addition to the amount of QDs in the beads, the color and intensity balances are affected by differences in the optical properties of different-sized QDs, and by the dependence of instrumental response on wavelength. However, all these factors can be compensated by varying the amounts of QDs for each emission color, and this allows empirical rules to be developed for preparing multicolor-tagged beads at predetermined intensity levels.

We note that additional studies are needed to quantitatively evaluate the uniformity of multicolor-encoded beads as well as the identification accuracies. The nearly perfect results shown for single-color

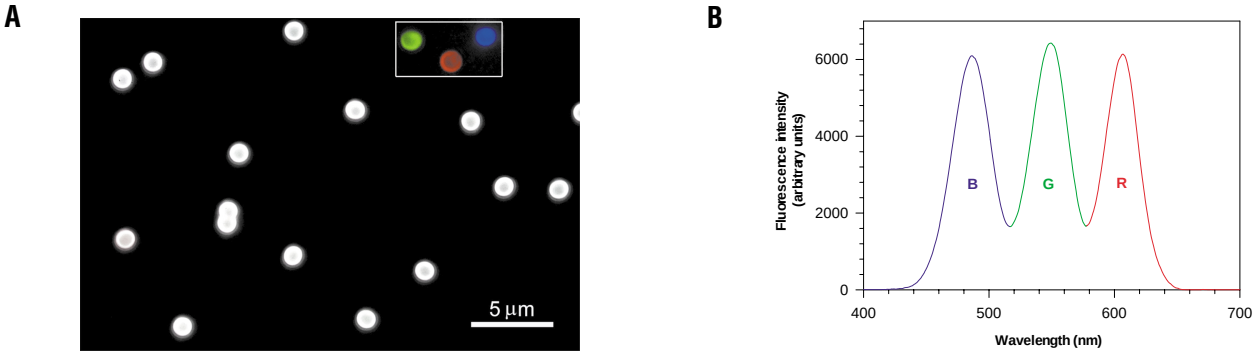

Figure 4. Multicolor QD-tagged beads with precisely controlled fluorescence intensities. (A) Fluorescence image of color-balanced beads. In the upper right corner, single-color beads were digitally inserted to show that this should not be mistaken as a black and white image. (B) Single-bead fluorescence spectrum, showing three separated peaks (484, 547, and 608 nm) with nearly equal intensities.

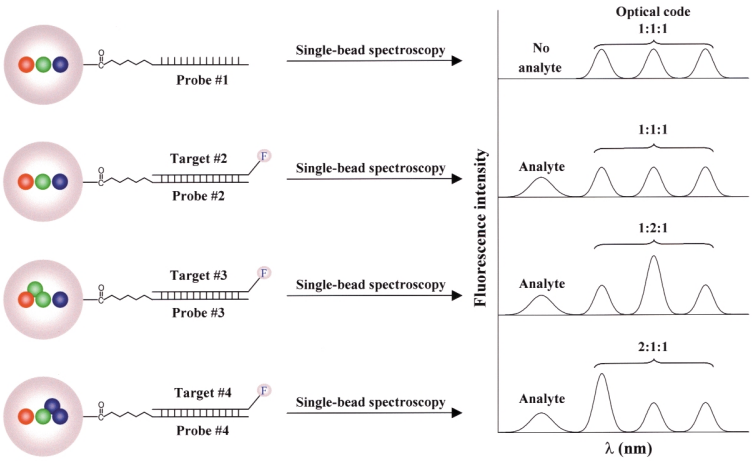

Figure 5. Schematic illustration of DNA hybridization assays using QD-tagged beads. Probe oligos (No. 1–4) were conjugated to the beads by cross-linking, and target oligos (No. 1–4) were detected with a blue fluorescent dye such as Cascade Blue. After hybridization, nonspecific molecules and excess reagents were removed by washing. For multiplexed assays, the oligo lengths and sequences were optimized so that all probes had similar melting temperatures (T_m = 66°–99°C) and hybridization kinetics (30 min). See legend in Figure 6 for the sequences used.

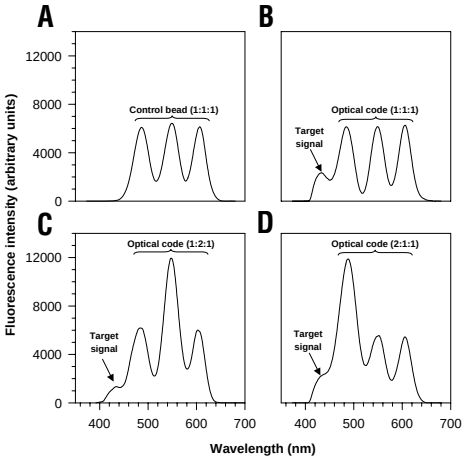

Figure 6. DNA hybridization assays using multicolor encoded beads. (A) Fluorescence signals obtained from a single bead with the code 1:1:1 (corresponding to probe 5′-TCA AGG CTC AGT TCG AAT GCA CCA TA-3′), after exposure to a control DNA sequence (3′-TGA TTC TCA ACT GTC CCT GGA ACA GA-5′). The control DNA was tagged with the same fluorophore as the target DNA. (B) Fluorescence signals of a single bead with the code 1:1:1 (same as in panel A), after hybridization with its target 5′-TAT GGT GCA TTC GAA CTG AGC CTT GA-3′. (C) Fluorescence signals of a single bead with the code 1:2:1 (corresponding to probe 5′-CCG TAC AAG CAT GGA ACG GCT TTT AC-3′), after hybridization with its target 5′-GTA AAA GCC GTT CCA TGC TTG TAC GG-3′. (D) Fluorescence signals of a single bead with the code 2:1:1 (corresponding to probe 5′-TAC TCA GTA GCG ACA CAT GGT TCG AC-3′), after hybridization with its target 5′-GTC GAA CCA TGT GTC GCT ACT GAG TA-3′.

beads (Fig. 3) will be more difficult to achieve with multicolor-encoded beads because of spectral and intensity overlapping problems. Still, the novel optical properties of QDs could be exploited to improve the multiplexed coding capabilities. For example, the QD fluorescence spectra are nearly symmetrical and can be modeled as a Gaussian distribution. With pre-set emission maxima and intensity levels, spectral deconvolution and signal processing methods should allow code identification under difficult conditions.

To demonstrate the use of QD-tagged beads for biological assays, we designed a model DNA hybridization system using oligonucleotide probes and triple-color encoded beads, as shown in Figure 5. Target DNA molecules are either directly labeled with a fluorescent dye or with a biotin (for binding to fluorescently tagged avidin). Optical spectroscopy at the single-bead level yields both the coding and the target signals. The coding signals identify the DNA sequence, whereas the target signal indicates the presence and the abundance of that sequence.

Several factors are important for optimizing the performance of this DNA hybridization assay. First, it is desirable to excite both the encoded bead and the labeled analyte with a single light source (single-excitation wavelength) for simplicity, convenience, and costs. For this reason, we used Cascade Blue to label the target oligos because this dye can be simultaneously excited with the embedded QDs at ~350 nm. Second, the analyte peak should be sufficiently separated from the coding signals to avoid spectral overlapping. Also, it may be necessary to use weak coding signals in order to detect the analyte signal at very low concentrations. Third, the optical properties of the embedded QDs must be stable under aqueous conditions and upon exposure to chemical and biochemical reagents. We solved this stability problem by sealing the porous beads with a thin polysilane layer, based on the procedures commonly used in bonded-phase chromatography[29]. Unlike free QDs in aqueous buffer, the embedded and protected QDs are stable in the temperature cycling conditions necessary for DNA hybridization assays.

Figure 6 shows the assay results of one mismatched and three complementary oligos hybridized to triple-color encoded beads. The code 1:1:1 corresponds to the oligo probe 5′-TCA AGG CTC AGT TCG AAT GCA CCA TA-3′. No analyte fluorescence was detected when control oligos (noncomplementary sequences) were used for hybridization (Fig. 6A). This result showed a high degree of sequence specificity and a low level of nonspecific adsorption. Analyte fluorescence signals were observed only in the presence of complementary targets, as shown in Figure 6B–D. Assuming 100% efficiencies for both probe conjugation and target hybridization, we estimated that each bead contained no more than 24,000 probe molecules and no more than 10,000 target molecules.

A limiting factor in target detection is likely to be spectral overlap with the coding signals. To minimize this spectral interference, it will be necessary to separate the coding and target signals as far as possible; for example, we are exploring the use of visible QDs for coding and near-infrared QDs for target labeling (R. Bailey, J. Strausburg, and S. Nie, unpublished data). Under complex biological conditions, we expect the performance (e.g., specificity and sensitivity) of our QD-tagged beads to be similar to that reported by Walt and co-workers[17–19]. In a recent paper, they used 3.1-μm encoded beads to study 25 sequences (including cancer and cystic fibrosis genes) and achieved a detection sensitivity of 10–100 fM target DNA (ref. 19). The underlying principles of nucleic acid hybridization and fluorescence detection are essentially the same, but multicolor QD coding should provide important advantages and applications not available with organic dyes.

In conclusion, we have reported a multiplexed coding technology based on the unique optical properties of semiconductor quantum dots. Imaging and spectroscopic measurements indicate that the single-color encoded beads are highly uniform and reproducible, yielding bead identification accuracies as high as 99.99% under favorable conditions. DNA hybridization studies have been demonstrated by using triple-color encoded beads, and the results show that the coding and target signals can be simultaneously read at the

single-bead level. We envision integrated bead-based assays using microfluidic devices in a serial fashion[30], or parallel binding assays using high-density microtiter plates[31]. In both formats, a library of encoded beads and recognition molecules (e.g., oligo probes and antibodies) will need to be developed, similar to the preparation of individual DNA clones for printing microarrays. Although this involves a significant amount of "front-end" work, such encoded beads should offer great flexibility in practical genomic and proteomic applications.

Experimental protocol

Bead synthesis and QD incorporation. Polystyrene beads were synthesized by using emulsion polymerization of styrene (98% vol/vol), divinylbenzene (1% vol/vol), and acrylic acid (1% vol/vol) at 70°C (refs 32,33). Transmission electron microscopy revealed that the beads had a 1.2-μm diameter with a standard deviation of 2–3% in size (diameter). Incorporation of QDs was achieved by swelling the beads in a solvent mixture containing 5% (vol/vol) chloroform and 95% (vol/vol) propanol or butanol, and by adding a controlled amount of ZnS-capped CdSe QDs to the mixture. For single-color coding with 10 intensity levels, the ratios of QDs to beads were in the range of 640 to 50,000. For multicolor coding, the amounts of QDs were adjusted experimentally to compensate for the different optical properties of different-colored dots. The embedding process was complete within ~30 min at room temperature. Using similar procedures, we also synthesized polymer beads in the size range of 0.1–5.0 μm and embedded them with luminescent QDs. The bead size was controlled by changing the amount of a stabilizer (polyvinylpyrrolidone, MW = 40,000) used in the synthesis. Before DNA conjugation, the encoded beads were protected by using 3-mercaptopropyl trimetroxysilane, which polymerized inside the pores upon addition of a trace amount of water.

Conjugation of oligo probes. Standard protocols were used to covalently attach the carboxylic acid groups on the bead surface to streptavidin molecules[34]. Nonspecific sites on the bead surface were blocked by using BSA (0.5 mg/ml) in PBS buffer (pH 7.4). Biotinylated oligo probes (26-mer oligonucleotides, 5′-biotin TEG, high-performance liquid chromatography–purified; TriLink Biotechnol., San Diego, CA) were linked to the beads via the attached streptavidin. 5′-Biotinylated target oligos were first labeled with avidin–Cascade Blue, and were then hybridized to the oligo probes in 0.1% sodium dodecyl sulfate PBS buffer at 40°C for 30 min. Before fluorescence measurement, the beads were cleaned by two rounds of centrifugation. Both sequential (one target at a time) and multiplexed (all targets together) assays yielded similar results.

Multicolor imaging. True-color fluorescence images were obtained with an inverted Olympus microscope (IX-70) and a digital color camera (Nikon DI). Broad-band excitation in the near-UV range (330–385 nm) was provided by a 100 W mercury lamp. A longpass dichroic filter (DM 400, Chroma Technologies, Brattleboro, VT) was used to reject the scattered light and to pass the Stokes-shifted fluorescence signals. A high-numerical-aperture (NA = 1.4, 100×), oil-immersion objective was used, and the total wide-field excitation power was ~5 mW.

Single-bead spectroscopy. Wavelength-resolved fluorescence spectroscopy was accomplished by using a fluorescence microscope (Nikon Diaphot) equipped with a single-stage spectrograph (Model 270M, Spex, Edison, NJ) and a thermoelectrically cooled charge-coupled device (CCD) detector (Princeton Instruments, Trenton, NJ). Near-UV excitation (330–385 nm) was provided by a 100 W mercury lamp.

Acknowledgments

We are grateful to Warren C.-W. Chan for help in quantum dot synthesis and for stimulating discussions. This work was supported in part by the National Institutes of Health and the Department of Energy. S.N. acknowledges the Whitaker Foundation for a Biomedical Engineering Award and the Beckman Foundation for a Beckman Young Investigator Award.

Received 14 May 2001; accepted 18 May 2001

1. Fodor, S.P.A. *et al.* Light-directed, spatially addressable parallel chemical synthesis. *Science* **251**, 767–773 (1991).
2. Schena, M., Shalon, D., Davis, R.W. & Brown, P.O. Quantitative monitoring of gene-expression patterns with a complementary-DNA microarray. *Science* **270**, 467–470 (1995).
3. Dickinson, T.A., Michael, K.L., Kauer, J.S. & Walt, D.R. Convergent, self-encoded bead sensor arrays in the design of an artificial nose. *Anal. Chem*. **71**, 2192–2198 (1999).
4. Clark, H.A., Hoyer, M., Philbert, M.A. & Kopelman, R. Optical nanosensors for chemical analysis inside single living cells: fabrication, characterization, and methods for intracellular delivery of PEBBLE sensors. *Anal. Chem*. **71**, 4831–4836 (1999).
5. Harrison, D.J. *et al.* Micromachining a miniaturized capillary electrophoresis-based chemical analysis system on a chip. *Science* **261**, 895–897 (1993).
6. Ramsey, J.M., Jacobson, S.C. & Knapp, M.R. Microfabricated chemical measurement systems. *Nat. Med*. **1**, 1093–1096 (1995).
7. Woolley, A.T. & Mathies, R.A. Ultra-high-speed DNA fragment separations using microfabricated capillary array electrophoresis chips. *Proc. Natl. Acad. Sci. USA* **91**, 11348–11352 (1994).
8. Alivisatos, A.P. Semiconductor clusters, nanocrystals, and quantum dots. *Science* **271**, 933–937 (1996).
9. Nirmal, M. & Brus, L.E. Luminescence photophysics in semiconductor nanocrystals. *Acc. Chem. Res.* **32**, 407–414 (1999).
10. Chen, J.W. *et al.* A microsphere-based assay for multiplexed single nucleotide polymorphism analysis using single base chain extension. *Genome Res*. **10**, 549–557 (2000).
11. Bruchez, M. Jr., Moronne, M., Gin, P., Weiss, S. & Alivisatos, A.P. Semiconductor nanocrystals as fluorescent biological labels. *Science* **281**, 2013–2015 (1998).
12. Chan, W.C.-W. & Nie, S.M. Quantum dot bioconjugates for ultrasensitive nonisotopic detection. *Science* **281**, 2016–2018 (1998).
13. Mitchell, G.P., Mirkin, C.A. & Letsinger R.L. Programmed assembly of DNA functionalized quantum dots. *J. Am. Chem. Soc.* **121**, 8122–8123 (1999).
14. Mattoussi, H. *et al.* Self-assembly of CdSe-ZnS quantum dots bioconjugates using an engineered recombinant protein. *J. Am. Chem. Soc*. **122**, 12142–12150 (2000).
15. Pathak, S., Choi, S.-K., Arnheim, N. & Thompson, M.E. Hydroxylated quantum dots as luminescent probes for *in situ* hybridization. *J. Am. Chem. Soc.* **123**, 4103–4104 (2001).
16. Fulton, R.J., McDade, R.L., Smith, P.L., Kienker, L.J. & Kettman, J.R. Jr. Advanced multiplexed analysis with the FlowMetrix (TM) system. *Clin. Chem*. **43**, 1749–1756 (1997).
17. Steemers, F.J., Ferguson, J.A. & Walt, D.R. Screening unlabeled DNA targets with randomly ordered fiber-optic gene arrays. *Nat. Biotechnol*. **18**, 91–94 (2000).
18. Ferguson, J.A., Boles, T.C., Adams, C.P. & Walt, D.R. A fiber-optic DNA biosensor microarray for the analysis of gene expression. *Nat.re Biotechnol*. **14**, 1681–1684 (1996).
19. Ferguson, J.A., Steemers, F.J. & Walt, D.R. High-density fiber-optic DNA random microsphere arrays. *Anal. Chem*. **72**, 5618–5624 (2000).
20. Mandecki, W., Ernst, E. & Kogan, N. Light-powered microtransponders for high multiplex-level analyses of nucleic acids. *Abstr. Pap. Am. Chem. Soc.* **219,** U755–U755, Part 1 (2000).
21. Moran, E.J. *et al.* Radio-frequency tag encoded combinatorial library method for the discovery of tripeptide-substituted cinnamic acid inhibitors of the protein-tyrosine-phosphatase PTP1B. *J. Am. Chem. Soc*. **117**, 10787–10788 (1995).
22. Hines, M.A. & Guyot-Sionnest, P. Synthesis and characterization of strongly luminescing ZnS-capped CdSe nanocrystals. *J. Phys. Chem*. **100**, 468–471 (1996).
23. Dabbousi, B.O. *et al.* (CdSe)ZnS core-shell quantum dots: synthesis and characterization of a size series of highly luminescent nanocrystallites. *J. Phys. Chem. B* **101**, 9463–9475 (1997).
24. Peng, X., Schlamp, M.C., Kadavanich, A.V. & Alivisatos, A.P. Epitaxial growth of highly luminescent CdSe/CdS core/shell nanocrystals with photostability and electronic accessibility. *J. Am. Chem. Soc.* **119**, 7019–7029 (1997).
25. Zhang, Y.-Z., Kemper, C.R. & Haugland, R.P. Microspheres with fluorescent spherical zones. US 5,786,219 (1998).
26. Kagan, C.R., Murray, C.B., Nirmal, M. & Bawendi, M.G. Electronic energy transfer in CdSe quantum dot solids. *Phys. Rev. Lett*. **76**, 1517–1520 (1996).
27. Micic, O.I., Jones, K.M., Cahill, A. & Nozik, A.J. Optical, electronic, and structural properties of uncoupled and close-packed arrays of InP quantum dots. *J. Phys. Chem. B* **102**, 9791–9796 (1998).
28. Prummer, M. *et al.* Single-molecule identification by spectrally and time-resolved fluorescence detection. *Anal. Chem*. **72**, 443–447 (2000).
29. Dorsey, J.G. & Cooper, W.T. Retention mechanisms of bonded-phase liquid-chromatography. *Anal. Chem*. **66**, 857A–867A (1994).
30. Fu, A.Y., Spence, C., Scherer. A., Arnold, F.H & Quake, S.R. A microfabricated fluorescence-activated cell sorter. *Nat. Biotechnol*. **17**, 1109–1111 (1999).
31. Miraglia. S. *et al.* Homogeneous cell- and bead-based assays for high throughput screening using fluorometric microvolume assay technology. *J. Biomol. Screening* **4**, 193–204 (1999).
32. Hermkens, P.H.H., Ottenheijm, H.C.J. & Rees, D. Solid-phase organic reactions: a review of the recent literature. *Tetrahedron* **52**, 4527–4554 (1996).
33. Yang, B.Z., Chen, L.W. & Chiu, W.Y. Effects of acrylic acid on number density of polymer particles in emulsifier-free emulsion copolymerization of styrene and acrylic acid. *Polymer J*. **29**, 737–743 (1997).
34. Hermanson, G.T. *Bioconjugate techniques.* (Academic Press, New York; 1996).